



MACH NUMBER EFFECTS ON AIRFOIL AEROACOUSTIC SOURCES AND NOISE PROPAGATION

João Luiz F. Azevedo

Instituto de Aeronáutica e Espaço, 12228-903, São José dos Campos, SP, Brazil
joaoluiz.azevedo@gmail.com

William R. Wolf

Universidade Estadual de Campinas, Faculdade de Engenharia Mecânica, 13083-970, Campinas, SP, Brazil
wolf@fem.unicamp.br

Sanjiva K. Lele

Stanford University, Stanford, CA, 94305-4035, USA
lele@stanford.edu

Abstract. *The present investigation of airfoil self-noise generation and propagation concerns the effects of mean flow and aeroacoustic sources on the broadband noise that arises from the interaction of turbulent boundary layers with the airfoil trailing edge and the tonal noise that arises from vortex shedding generated by laminar boundary layers. Compressible large eddy simulations (LES) are conducted for a NACA0012 airfoil with rounded trailing edge for two flow configurations with different freestream Mach numbers, $M = 0.115$ and $M = 0.4$. The Reynolds number based on the airfoil chord is fixed at $Re = 408,000$. The acoustic predictions are performed by the Ffowcs Williams and Hawkings (FWH) acoustic analogy formulation and incorporate convective effects. For low Mach number flows, quadrupole sources can be neglected in the FWH equation and mean flow effects appear only for high frequencies. However, for higher speeds, convection effects are relevant for all frequencies and quadrupole sources have a more pronounced effect for medium and high frequencies. The convective effects are most readily observed in the upstream direction.*

Keywords: *Mach number effects, Aeroacoustics, Airfoil noise, LES, Tonal and broadband noise*

1. INTRODUCTION

Airfoil trailing edge noise is one of the fundamental airframe noise mechanisms (Lockard and Lilley, 2004) and understanding the physics associated with its generation and propagation is of paramount importance for the design of low-noise aerodynamic shapes such as wings and high-lift devices, as well as wind turbine blades, propellers and fans. Airfoil noise originates from the unsteady flow past an airfoil configuration and Brooks *et al.* (1989) identify five physical mechanisms associated with airfoil self-noise generation, namely laminar and turbulent boundary layer noise, trailing edge bluntness noise, separation-stall noise and tip vortex noise.

Numerical simulation of airfoil noise is a relatively new research topic. Among the first numerical investigations of trailing edge noise, one can cite the work by Wang and Moin (2000), Singer *et al.* (2000) and Manoha *et al.* (2000). Wang and Moin (2000) and Manoha *et al.* (2000) used incompressible large eddy simulation (LES) to compute the unsteady near flowfield responsible for the sound generation processes. The acoustic analogy of Ffowcs-Williams and Hall (1970) was used for far-field sound predictions of a Blake profile (Wang and Moin, 2000) and of a thick flat plate (Manoha *et al.*, 2000). The latter also used the acoustic analogy formulation of Curle (1955) to predict far-field sound. Singer *et al.* (2000) solved the unsteady Reynolds-averaged Navier Stokes (URANS) equations and the Ffowcs-Williams and Hawkings (1969)(FWH) acoustic analogy formulation to predict the sound generated by a bluff body vortex generator positioned close to the sharp trailing edge of an airfoil. Recently, several authors have investigated the problem of trailing edge noise generation and propagation using computational simulations. Sandberg *et al.* (2008), Sandberg *et al.* (2009), Jones *et al.* (2010) and Jones and Sandberg (2010) conducted direct numerical simulations (DNS) of turbulent flows at moderate Reynolds numbers past NACA0006 and NACA0012 airfoils at different angles of incidence. They have investigated several mechanisms of airfoil sound generation to identify potential sources of noise and they have also studied the application and accuracy of Amiet's theory (Amiet, 1976) to predict far-field sound using the computed hydrodynamic DNS data.

However, several previous studies of airfoil noise used incompressible LES. Such approach restricted the application of the unsteady surface pressures, directly computed by LES, to acoustic analogy formulations only in the low frequency regime. For these incompressible simulations, the scattered acoustic pressure for non-compact bodies can be computed through the accurate calculation of the quadrupole sources as shown by Oberai *et al.* (2002) and Khalighi *et al.* (2010). Other limitations of some previous investigations include insufficient near-wall resolution for the meshes used, application of low-order schemes and insufficient domain sizes. The present study particularly addresses the accurate prediction the

noise spectra and, thus, enables a detailed examination of processes controlling the spectral amplitudes and directivity, in particular at high frequencies. Hence, the present investigation primarily concerns the broadband noise that arises from the interaction of turbulent boundary layers with the airfoil trailing edge. Some aspects of trailing edge noise generation and propagation not covered, or not fully understood, in the literature are addressed in the paper. In particular, the effects of mean flow convection on sound directivity and the role of dipoles and quadrupoles for low and moderate Mach numbers for different frequency ranges are addressed.

2. THEORETICAL AND NUMERICAL FORMULATION

The general curvilinear form of the compressible Navier-Stokes equations is solved using LES in the present paper. The current numerical capability applies a high-order accurate non-dissipative compact scheme. The numerical scheme for spatial discretization is a sixth-order accurate compact scheme (Nagarajan *et al.*, 2003) implemented on a staggered grid. The current numerical capability allows the use of overset grids with a fourth-order accurate Hermitian interpolation between grid blocks (Bhaskaran and Lele, 2010). The time integration of the fluid equations is carried out by a fully implicit second-order Beam-Warming scheme (Beam and Warming, 1978) in the near-wall region in order to overcome the time step restriction that would otherwise appear with the use of an explicit method. A third-order Runge-Kutta scheme is used for time advancement of the equations in flow regions far away from solid boundaries. No-slip adiabatic wall boundary conditions are applied along the solid surfaces except for the tripping region where suction and blowing are applied. In the simulations here discussed, boundary layers are tripped by steady suction and blowing. The tripping methodology is applied in order to force transition to turbulent boundary layers and it is chosen to model the experimental tripping used by Brooks *et al.* (1989) for similar flow configurations. Characteristic plus sponge boundary conditions are applied in the farfield locations and periodic boundary conditions are applied in the spanwise direction. The dynamic subgrid model formulation of Lilly (1992) is used to include the effects of unresolved turbulent scales. The numerical tool has been previously validated for several compressible flow simulations (Bhaskaran and Lele, 2010; Nagarajan *et al.*, 2007; Wolf and Lele, 2012; Wolf *et al.*, 2012).

The acoustic predictions are performed by the FWH acoustic analogy formulation (Ffowcs-Williams and Hawkings, 1969). The frequency domain formulation presented by Lockard (2000) is implemented and incorporates convective effects. Surface dipole integrations are computed along the airfoil surface and a Hanning filter is applied in an energy preserving manner (Lockard, 2000) to dipole sources before they are transformed to the frequency domain. Volume integrations of quadrupole source terms appearing in the FWH equation are performed using the 3-D convective wideband multi-level adaptive fast multipole method (FMM) developed by Wolf and Lele (2011a,b) to reduce the computational cost of the calculation of aeroacoustic integrals in the FWH formulation. The NACA 0012 airfoil geometry is chosen due to the large experimental and computational data set available in the literature. Additional validation of the simulation capability here discussed is presented in Wolf *et al.* (2012). In the present study, attention is directed towards the effects of mean flow and quadrupole source effects on sound propagation through the comparison of directivity plots obtained for various frequencies and through plots of sound pressure level spectra computed at different observer locations.

3. RESULTS

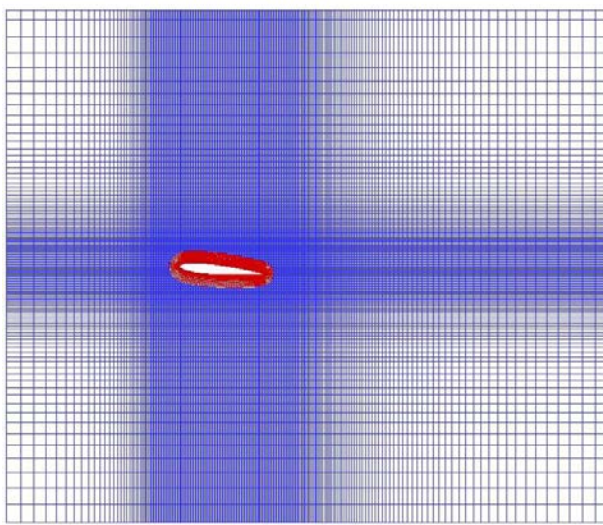
Numerical simulations are conducted for a NACA0012 airfoil with rounded trailing edge, and the aerodynamic and aeroacoustic results obtained by LES and the FMM-FWH formulation are discussed in this section. Two flow configurations are addressed here, and these are described in Table 1. The comparison of these two test cases, which are identical except for the freestream Mach number, attempts to highlight the effects of mean flow convection on sound directivity.

Table 1. Summary of flow configurations analyzed. Here, Re_c is the Reynolds number based on the airfoil chord, M_∞ is the freestream Mach number, Δt is the dimensionless time step for time marching of the LES equations.

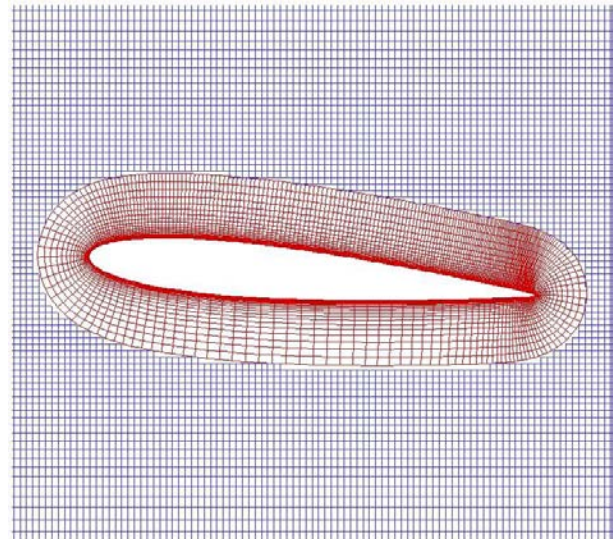
Configuration	Re_c	M_∞	AoA	B.L. Tripping	Δt
1	408,000	0.115	5 deg.	suction side	0.0004
2	408,000	0.4	5 deg.	suction side	0.0001

3.1 Configuration 1: $M_\infty = 0.115$, $Re_c = 408,000$, AoA = 5 deg.

Configuration 1 comprises the study of sound generated by the turbulent and laminar boundary layers convected past the rounded trailing edge of a NACA0012 airfoil at five degrees of angle of incidence. The flow Reynolds number based on the airfoil chord is set $Re_c = 408,000$ and the freestream Mach number is $M_\infty = 0.115$. The boundary layer is tripped only on the suction side of the NACA0012 airfoil by steady suction, performed over the region $0.15 < x/c < 0.175$, and blowing, over the region $0.175 < x/c < 0.20$. The magnitude of steady suction and blowing is constant over



(a) Full view of computational grid (every 4-th grid point shown).



(b) Detail view of O-grid around airfoil region (every 4-th grid point shown).

Figure 1. Mesh details for simulation of turbulent flow past a NACA0012 airfoil at $\text{AoA} = 5 \text{ deg.}$, $M_\infty = 0.115$ and $Re_c = 408,000$.

$0.01 < z/c < 0.09$ with $|U_{blowing}| = |U_{suction}| = 0.03U_\infty$.

Mesh generation for all test cases analyzed in the present work have addressed all the required issues to guarantee the necessary quality in order to capture the physical mechanisms responsible for sound generation. The present grid configuration consists of a symmetric body-fitted O-grid block and a Cartesian background grid block. The body-fitted O-grid block is composed of $960 \times 125 \times 128$ nodes, in the periodic, wall normal and spanwise directions, respectively, that accurately resolve the turbulent boundary layers. The Cartesian background grid block has $896 \times 511 \times 64$ nodes, in the streamwise, transversal and spanwise directions, respectively, with uniform resolution around the O-grid block and that gently stretches out to the farfield regions. In Figs. 1 (a) and (b), one can see the full view of the computational grid and a detail of the O-grid around the airfoil region, respectively. The spanwise width of the numerical simulation is $L_Z = 0.1c$ and the mesh distribution along the airfoil span is uniform with $\Delta z = 0.1c/128$. Previous work by the present authors (Wolf *et al.*, 2012) has demonstrated that the spanwise coherence of the surface pressure on the upper surface of the aerofoil drops considerably for all frequencies studied and for source regions separated by L_Z . This means that source regions separated by such distance radiate sound independently from neighbouring sources in a statistical sense and, therefore, the spanwise domain is sufficiently long for the present purposes.

The overset grids are carefully designed to capture the turbulent boundary layers and wake at an affordable computational cost. Maximum values of grid spacing along the wall region in terms of wall units are given by $\Delta x^+ \approx 50$, $\Delta y^+ \approx 0.5$ and $\Delta z^+ \approx 20$ and they occur at the flow transition region at $x/c \approx 0.3$. At the trailing edge region, $0.8 < x/c < 1.0$, values of grid spacing in terms of wall units are given by $\Delta x^+ \approx 10$, $\Delta y^+ \approx 0.3$ and $\Delta z^+ \approx 10$. For the present grid configuration, span-averaged values of μ_{SGS} along the airfoil turbulent boundary layers reach peak values of $\mu_{SGS} \approx 0.1\mu_\infty$. More details on this issue can be seen in Wolf (2011). It is true that, for such low values of μ_{SGS} , the subgrid model could actually be turned off without any significant changes in the flow solutions obtained. However, this is an observation which one arrives at only after the simulation has been run.

For this configuration, a laminar boundary layer develops along the pressure side of the airfoil due to the favorable pressure gradient and since tripping is only applied on the suction side. Figure 2 (a) shows wall pressure power spectral densities normalized by outer variables, at different chord locations on the suction side of the airfoil. These are similar to the zero degree angle of incidence case results, discussed in Wolf *et al.* (2012), and broadband spectra are observed over the suction side of the airfoil. This figure also shows a plot of wall pressure power spectral density measured at $x/c = 0.95$ on the pressure side of the airfoil. One can see a narrow band peak at non-dimensional frequency $\omega\delta^*/U_e \approx 0.55$ (Helmholtz number $kc \approx 9$) due to vortex shedding from the laminar boundary layer. Figure 2 (b) presents similar results using a different normalization of the results.

Numerical acoustic predictions are compared to experimental data provided by Brooks *et al.* (1989). In the experiments, the flow Reynolds and Mach numbers are $Re_c = 408,000$ and $M_\infty = 0.115$, and the airfoil angle of incidence is $\text{AoA} = 10.8 \text{ deg.}$ One should mention that flow curvature and downwash deflection are different in the wind tunnel experiment and in an ideal undisturbed freestream flow and, therefore, Brooks *et al.* (1989) used lifting surface theory to develop a wind tunnel correction to the airfoil angle of incidence. An airfoil with the corrected angle of incidence in an undisturbed freestream should provide the same lift as an airfoil with the actual wind tunnel angle of incidence. For the

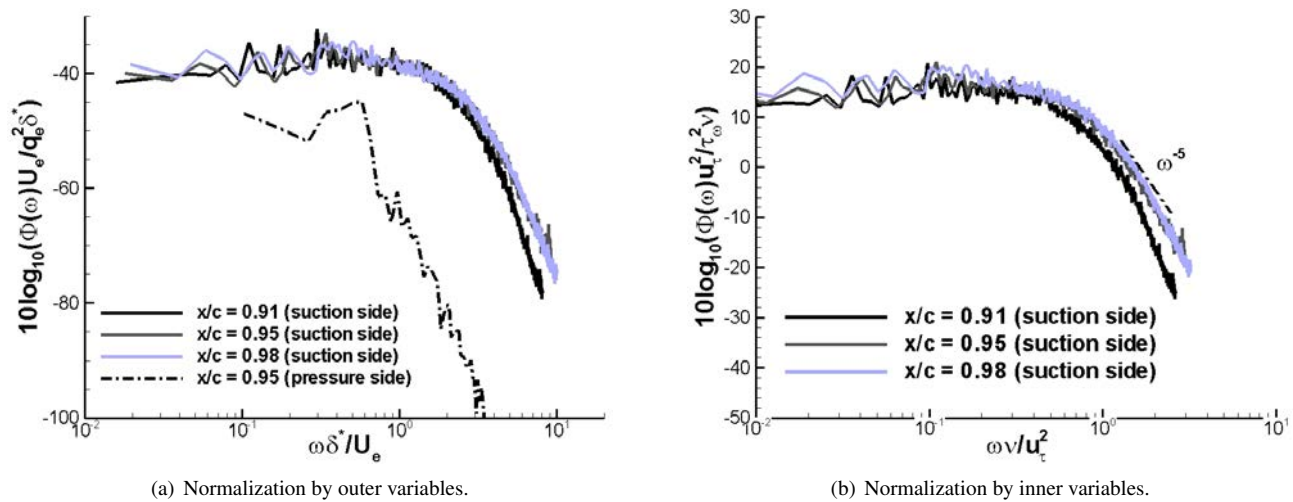


Figure 2. Wall pressure power spectral densities at different airfoil chord locations for configuration 1.

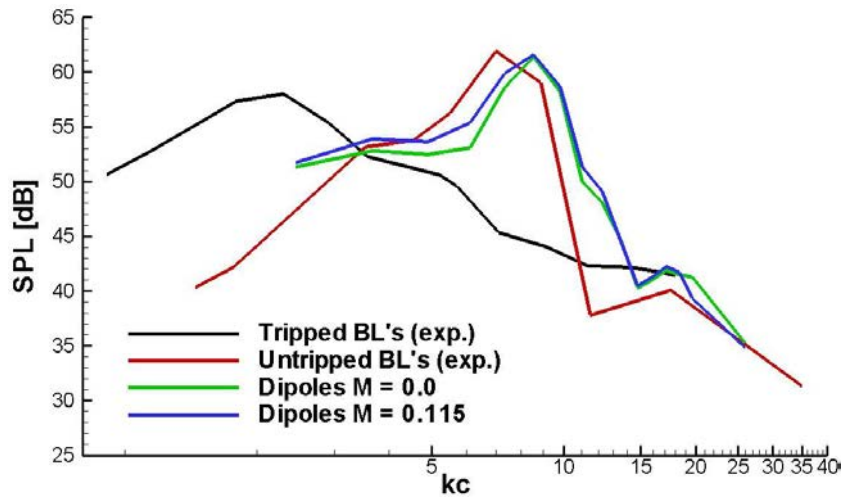
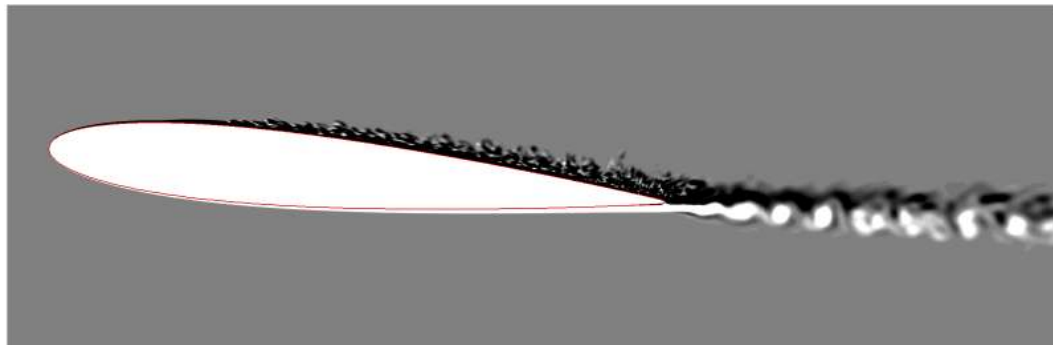


Figure 3. Sound pressure level at observer location $x = c$, $y = 7.9c$ and mid-span for configuration 1.

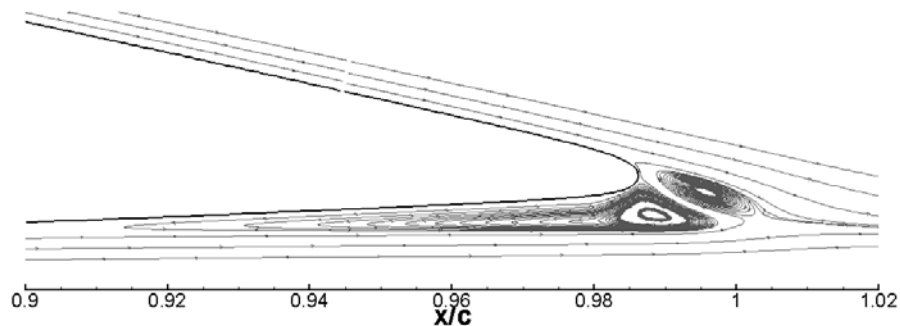
present configuration, the corrected angle of incidence is $\text{AoA} = 5.4$ deg. Therefore, the present comparison between Brooks *et al.* (1989) experimental data and the current simulations can be regarded as reasonable.

In Fig. 3, one can observe a comparison of sound pressure level between the predictions for configuration 1 and experiments for a microphone positioned at $x = c$, $y = 7.9c$ and mid-span. It should be emphasized that, although the peak energy levels calculated along the pressure side of the airfoil are lower than those observed on the suction side, as shown in Fig. 2, the same is not true when the SPL is concerned. Figure 3 corroborates this observation as the peak frequency occurs at $kc \approx 9$, which correlates with the vortex shedding frequency. Experimental acoustic measurements are shown for tripped and untripped boundary layers. In the experiment, when the boundary layers are not tripped, the suction side of the airfoil develops a turbulent boundary layer due to the adverse pressure gradient. However, a laminar boundary layer is developed along the pressure side due to the favorable pressure gradient. As discussed, the numerical simulation for configuration 1 uses the tripping mechanism along the suction side of the airfoil in order to develop a turbulent boundary layer. Therefore, the flow configuration is similar to that from the untripped experiment. Furthermore, one should note that the present simulations consider a rounded trailing edge, as previously explained, whereas the experiment is performed for a “sharp” trailing edge model, as reported by Brooks *et al.* (1989). It is clear that the experimental model must have some finite thickness at the airfoil trailing edge due to obvious construction issues, but the trailing-edge thickness is not provided in the reference. Hence, considering the small differences which exist between experimental and simulated configurations, the present acoustic prediction actually shows a remarkably good agreement with the experimental data.

One can observe in Fig. 3 that there is a small frequency shift between the peaks in SPL for the experimental and numerical results. As discussed, the existence of this peak is associated to vortex shedding from the laminar boundary layer on the airfoil pressure side. Direct evidence of vortex shedding can be seen in Fig. 4 (a), which shows spanwise-averaged contours of the z -Cartesian component of vorticity. The turbulent character of the suction side boundary layer



(a) Spanwise-averaged z-vorticity.



(b) Recirculation bubble.

Figure 4. Spanwise vorticity along airfoil and wake regions and enlarged view of mean flow streamlines along trailing edge region for configuration 1.

as well as the laminar behavior of the pressure side flow are evident in this figure. Moreover, the shed vortices are also clearly seen downstream of the trailing edge, thus justifying the tonal noise observed in Fig. 3. It is interesting that a similar peak is shown in the experimental measurements, and Brooks *et al.* (1989) also attribute this peak to the vortex shedding from the pressure side laminar boundary layer. Further demonstration of the vortex shedding can be seen in Fig. 4 (b), which shows an enlarged view of the mean flow streamlines in the trailing edge region where a recirculation bubble develops.

In Figs. 5 and 6, the directivity plots and the acoustic near fields for different frequencies for configuration 1 are shown. Directivity plots, Fig. 5, are computed for observer locations at mid-span and $7.9c$ distant from the airfoil trailing edge. Only surface dipole sources are included in the FMM-FWH formulation. As one can notice, these plots are not symmetric since the airfoil is at 5 deg. angle of incidence. Moreover, the results show that noise radiation below the airfoil is more intense. In Fig. 6 it is clear that acoustic waves are generated at the trailing edge. Despite the low freestream Mach number, convection effects are important for mid- and high-frequencies. These effects are evident in Fig. 5, where one can see that acoustic pressure of high-frequency upstream lobes are amplified when mean flow effects are present in the FWH formulation. In this figure, it is important to observe the difference between the amplitude of acoustic pressure of the vortex shedding tone in Fig. 5 (b) and the amplitudes for the other frequencies. In Figs. 5 (c) and (d), the directivity plots are presented with different scales compared to Figs. 5 (a) and (b) for purposes of better visualization. The upstream amplification of the radiated noise by convective effects for intermediate to high frequencies is consistently observed for this configuration.

3.2 Configuration 2: $M_\infty = 0.4$, $Re_c = 408,000$, $AoA = 5$ deg.

Configuration 2 allows a study of the effects of a higher freestream Mach number on the sound generated by the turbulent and laminar boundary layers convected past the rounded trailing edge of a NACA0012 airfoil. The flow Reynolds number based on the airfoil chord is set at $Re_c = 408,000$, as in the previous case, but the freestream Mach number is $M_\infty = 0.4$ and the angle of incidence is set at five degrees. The boundary layer is tripped following the same procedure described for case 1 and the present grid configuration is also identical to that used in case 1. Hence, maximum values of grid spacing in terms of wall units are similar to that test case.

Figure 7 shows iso-surfaces of vorticity magnitude colored by streamwise momentum and a background slice with dilatation contours in gray scale for configurations 1 and 2. The upper surface turbulent boundary layers and wake structures are similar for both configurations. However, one can see that higher frequencies are present in the dilatation

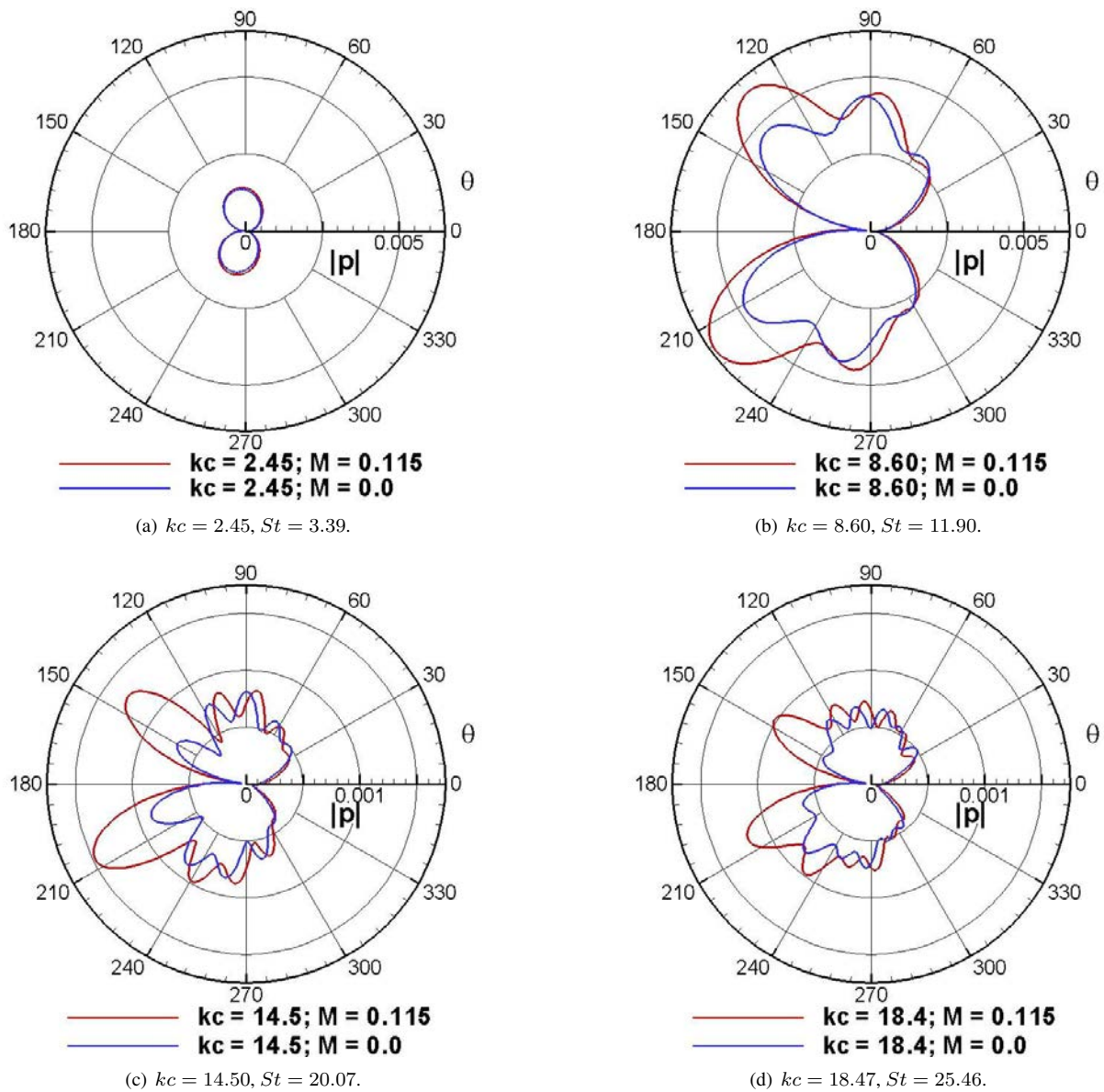


Figure 5. Directivity plots for observer locations at $r = 7.9c$ from the trailing edge for configuration 1.

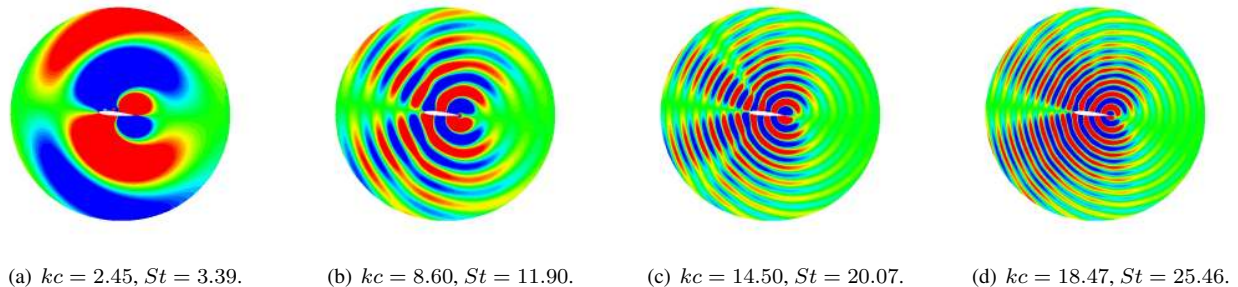


Figure 6. Acoustic near fields for configuration 1.

contours in Figure 7 (b) due to the higher freestream Mach number. A further detailed analysis in terms of aerodynamic results for configuration 1 can be found in Wolf (2011). Figure 8 (a), which shows spanwise-averaged contours of the z -Cartesian component of vorticity, confirms the occurrence of vortex shedding. An enlarged view of the mean flow streamlines at the trailing edge region, shown in Fig. 8 (b), give an indication of the size of the recirculation bubble for configuration 2.

Acoustic predictions for configuration 2 use the same approach described for configuration 1. They include the con-

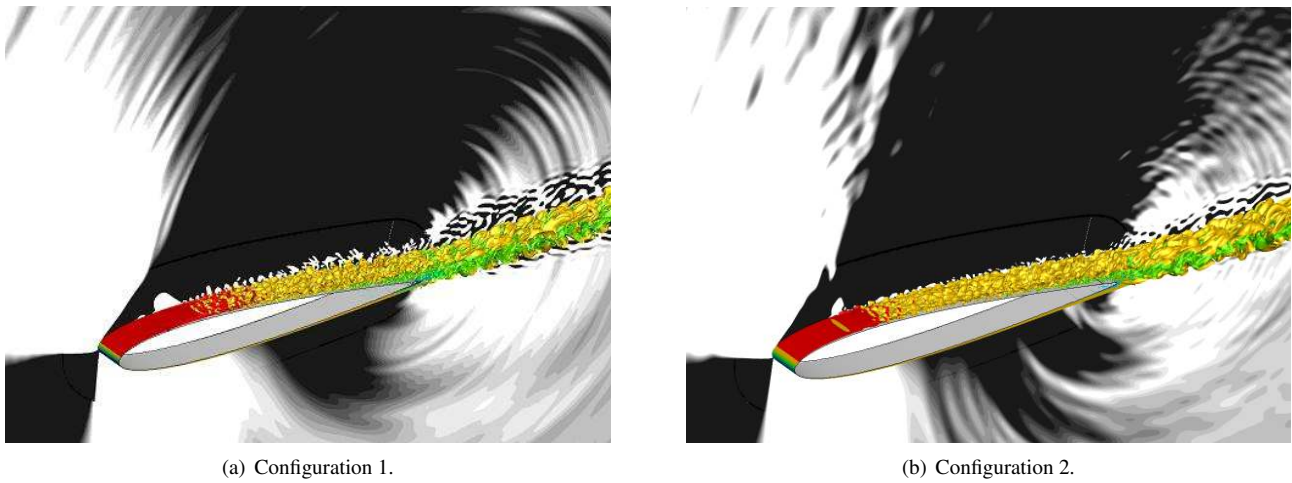
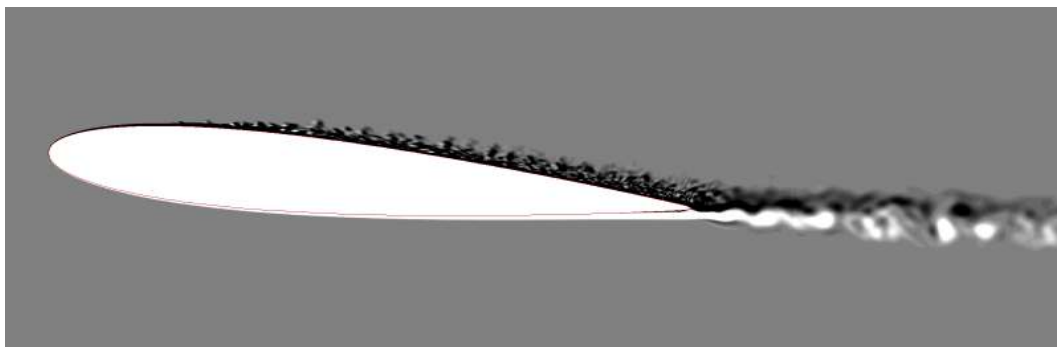
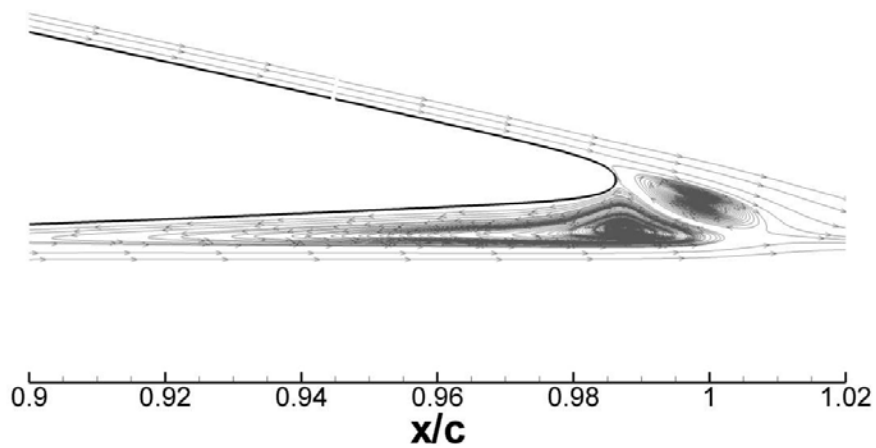


Figure 7. Iso-surfaces of vorticity magnitude colored by streamwise momentum with contours of dilatation in the background.



(a) Spanwise-averaged z-vorticity.



(b) Recirculation bubble.

Figure 8. Spanwise vorticity along airfoil and wake regions and enlarged view of mean flow streamlines along trailing edge region.

J.L.F. Azevedo, W.R. Wolf and S.K. Lele
Mach Number Effects on Airfoil Aeroacoustic Sources and Noise Propagation

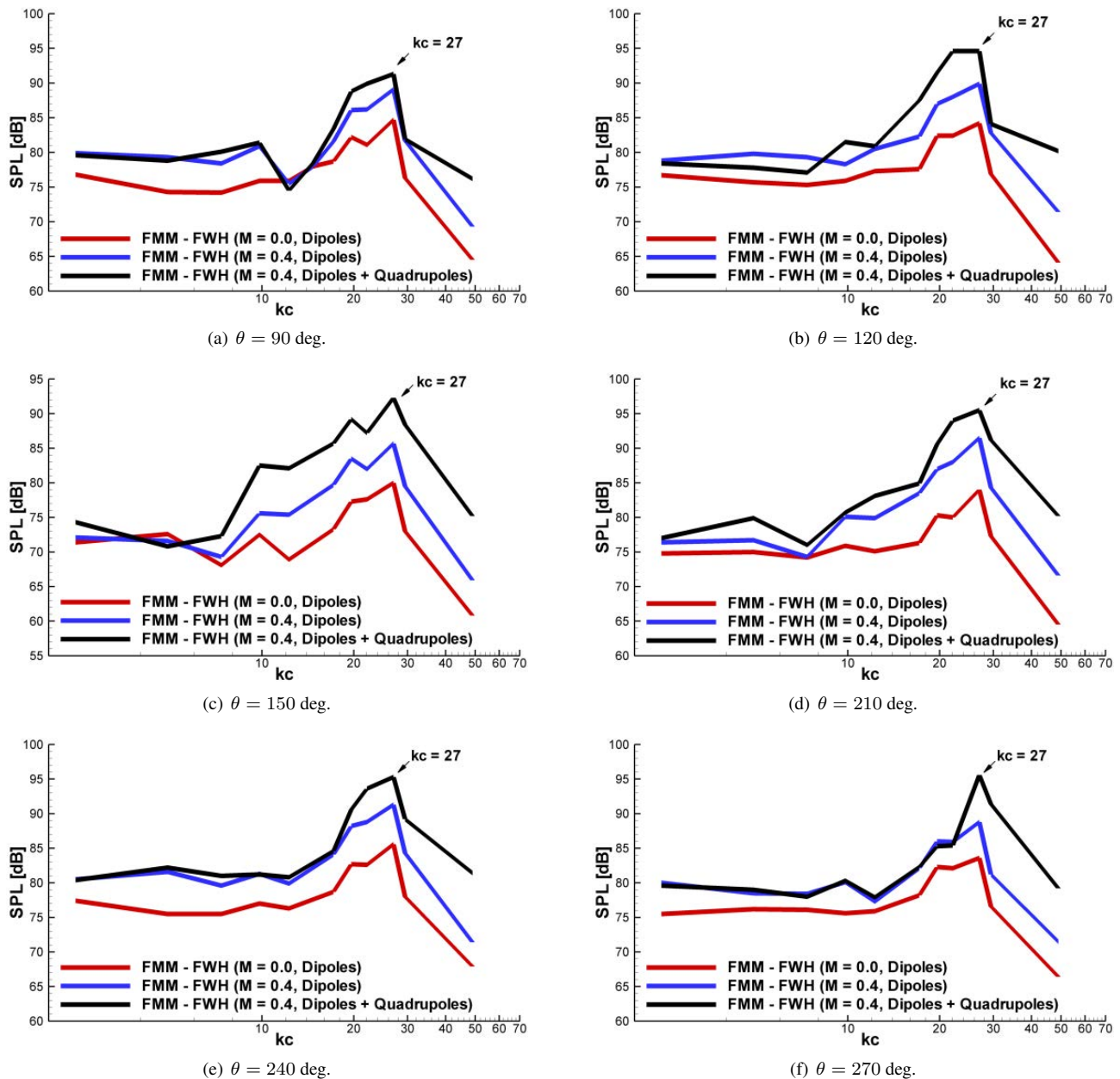


Figure 9. Sound pressure levels at observer locations at $r = 7.9c$.

tributions of both dipoles and quadrupoles, since, in this case, one expects that the volumetric sources should play a significant role in the sound generation. The procedure for the calculation of the frequency domain source terms is also identical to that used for configuration 1. However, for the present configuration, the non-dimensional time step used is $\Delta t = 0.0001$ and the sampling frequency is $F_s = 200$ dimensionless frequency units, which means that one flow snap shot is stored at every 0.005 dimensionless time units. Differently from the previous test case, before collecting data, the simulations are advanced in time over 15 airfoil flow-through times and data is collected over 2 additional airfoil flow-through times.

Figure 9 shows sound pressure levels at $r = 7.9c$, and $\theta = 90, 120, 150, 210, 240$ and 270 for $z = \text{mid-span}$. One can observe a tonal noise peak in the numerical prediction due to vortex shedding from the laminar boundary layer at $kc \approx 27$ for all microphone locations. In the figures, one can also assess the effects of mean flow and non-linear quadrupole sources. Mean flow effects have a tendency to shift the SPL by approximately 5 dB for all frequencies and observer angles $\theta = 90, 120, 240$ and 270 . For observer angles $\theta = 150$ and 210 , mean flow effects show less pronounced effects for lower frequencies but, again, shift the SPL for higher frequencies. Quadrupole sources present significant effects at medium and high frequencies for all observer positions. One can observe a shift of up to 5 dB in Fig. 9 due to quadrupole sources. When both mean flow effects and quadrupole sources are included in the FWH formulation, the SPL is shifted by up to 10 dB for some observer locations at medium and high frequencies, including the vortex shedding tonal peak region.

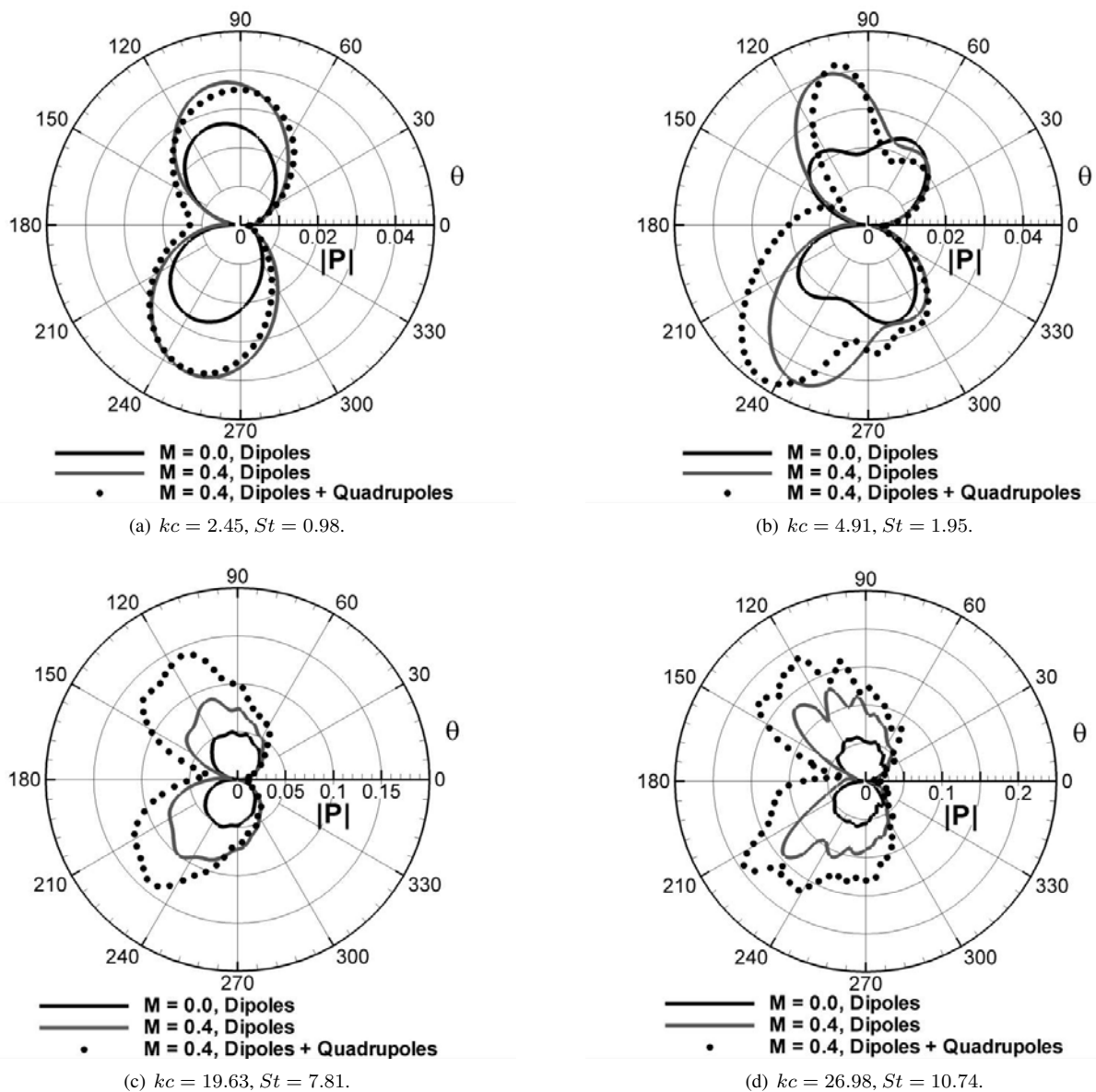


Figure 10. Directivity plots for observer locations at $r = 7.9c$ from the trailing edge for configuration 2.

Therefore, it is evident that these effects are important for the present flow configuration. While the mean flow effects increase the SPL for all frequencies for most selected observer locations, the quadrupole sources have a more pronounced effect for medium and high frequencies.

In Fig. 10, one can observe the directivity plots for different frequencies predicted at observer locations at mid-span and $7.9c$ distance from the airfoil trailing edge. The corresponding acoustic fields computed by the FMM-FWH formulation are shown in Fig. 11. Dipole and quadrupole sources are included for both figures. The directivity plots show the effects of convection and quadrupole sources. In the upstream direction, the effects of mean flow are significant for all directivity plots shown. However, the effects of quadrupoles are not important up to $kc = 2.45$, but they become increasingly relevant for higher frequencies.

4. CONCLUDING REMARKS

The present investigation of airfoil trailing edge noise generation and propagation concerns the broadband noise that arises from the interaction of turbulent boundary layers with the airfoil trailing edge and the tonal noise that arises from vortex shedding generated by laminar boundary layers and trailing edge bluntness. Compressible large eddy simulations (LES) are conducted for a NACA0012 airfoil with rounded trailing edge for two flow configurations with different freestream Mach numbers. The Reynolds number based on the airfoil chord is fixed at $Re_c = 408,000$. The acoustic predictions are performed by the Ffowcs Williams & Hawkins (FWH) acoustic analogy formulation and incorporate convective effects. Surface and volume integrations of dipole and quadrupole source terms appearing in the FWH equa-

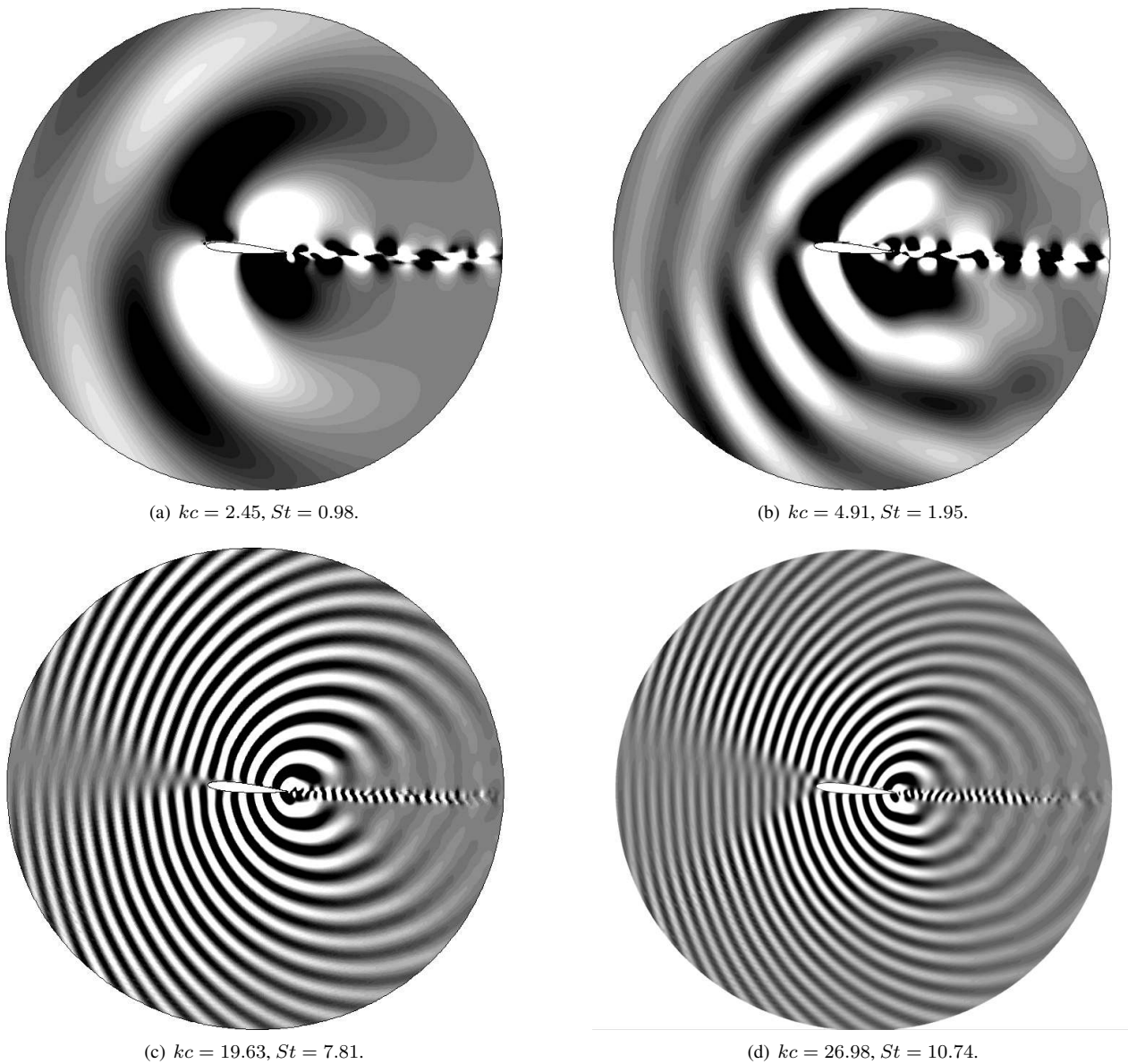


Figure 11. Acoustic near fields for configuration 2.

tion are performed using a 3-D wideband multi-level adaptive fast multipole method (FMM) in order to accelerate the calculations of aeroacoustic integrals.

The second configuration investigated ($M_\infty = 0.4$, $\text{AoA} = 5^\circ$, $\text{Re}_c = 408,000$) uses a similar boundary layer tripping as case 1. However, for this case, the freestream Mach number is increased and an assessment of mean flow and quadrupole source effects is provided. It is observed that mean flow effects are important at this higher Mach number at all frequencies. Predicted sound pressure levels are shifted by approximately 5 dB at all frequencies for observer angles normal to the flow direction. For upstream observer angles, mean flow effects are less pronounced for lower frequencies but, again, considerably shift the SPL for higher frequencies. The trends observed in the present work with regard to mean flow effect on directivity are in agreement with experimental results reported by Hutcheson and Brooks (2004). Quadrupole sources present significant effects at medium and high frequencies for all observer positions. One can observe an increase of up to 5 dB due to quadrupole sources. Therefore, when both mean flow effects and quadrupole sources are included in the FWH formulation, values of SPL are shifted by up to 10 dB for some observer locations at medium and high frequencies. Hence, while the mean flow effects increase the SPL for all frequencies for most observer locations, the quadrupole sources have a more pronounced effect for medium and high frequencies.

Hence, an important conclusion from the present work is that there is a significant influence of the mean flow on acoustic pressure directivity. It is typically expected that, for low speeds, there would be no important effect of convection on airfoil noise propagation. However, the work has shown that this is only true for low frequencies. For medium and high frequencies, convection effects are very important even for low Mach number flows. These effects are more pronounced

at upstream observation angles. As expected, quadrupole sources are not relevant for farfield noise predictions at low freestream Mach numbers. On the other hand, for moderate Mach numbers, quadrupole sources present significant effects at medium and high frequencies.

5. ACKNOWLEDGEMENTS

The authors acknowledge the financial support received from FAPESP under Grants No. 2011/12493-6 and No. 2013/07375-0, and from CNPq under Grants No. 312064/2006-3 and No. 471592/2011-0. The computational resources provided by the National Science Foundation are also gratefully acknowledged. The authors further acknowledge the following award for providing computing resources that have contributed to the research results reported within this paper: MRI-R2: Acquisition of a Hybrid CPU/GPU and Visualization Cluster for Multidisciplinary Studies in Transport Physics with Uncertainty Quantification. Finally, the authors also kindly acknowledge the financial support received from GE during the initial stages of the present work.

6. REFERENCES

- Amiet, R.K., 1976. "Noise due to turbulent flow past a trailing edge". *Journal of Sound and Vibration*, Vol. 47, pp. 387–393.
- Beam, R.M. and Warming, R.F., 1978. "An implicit factored scheme for the compressible Navier-Stokes equations". *AIAA Journal*, Vol. 16, pp. 393–402.
- Bhaskaran, R. and Lele, S.K., 2010. "Large eddy simulation of free-stream turbulence effects on heat transfer to a high-pressure turbine cascade". *Journal of Turbulence*, Vol. 11, pp. 1–15.
- Brooks, T.F., Pope, D.S. and Marcolini, M.A., 1989. "Airfoil self-noise and prediction". Technical Report 1218, NASA Reference Publication.
- Curle, N., 1955. "The influence of solid boundaries upon aerodynamic sound". *Journal of Fluid Mechanics*, Vol. 231, pp. 505–514.
- Ffowcs-Williams, J.E. and Hall, L.H., 1970. "Aerodynamic sound generation by turbulent flow in the vicinity of a scattering half plane". *Journal of Fluid Mechanics*, Vol. 40, pp. 657–670.
- Ffowcs-Williams, J.E. and Hawkings, D.L., 1969. "Sound generation by turbulence and surface in arbitrary motion". *Philosophical Transaction of the Royal Society of London, Series A, Mathematical and Physical Sciences*, Vol. 264, pp. 321–342.
- Hutcheson, F.V. and Brooks, T.F., 2004. "Effects of angle of attack and velocity on trailing edge noise". *AIAA Paper 2004-1031*.
- Jones, L.E. and Sandberg, R.D., 2010. "Numerical investigation of airfoil self-noise reduction by addition of trailing-edge serrations". *AIAA Paper 2010-3703*.
- Jones, L.E., Sandham, N.D. and Sandberg, R.D., 2010. "Acoustic source identification for transitional airfoil flows using cross correlations". *AIAA Journal*, Vol. 48, pp. 2299–2312.
- Khalighi, Y., Mani, A., Ham, F. and Moin, P., 2010. "Prediction of sound generated by complex flows at low Mach numbers". *AIAA Journal*, Vol. 48, pp. 306–316.
- Lilly, D.K., 1992. "A proposed modification of the Germano subgrid-scale closure method". *Physics of Fluids*, Vol. 4, pp. 633–635.
- Lockard, D.P., 2000. "An efficient, two-dimensional implementation of the Ffowcs Williams and Hawkings equation". *Journal of Sound and Vibration*, Vol. 229, pp. 897–911.
- Lockard, D.P. and Lilley, G.M., 2004. "The airframe noise reduction challenge". Technical Report 213013, NASA Report.
- Manoha, E., Troff, B. and Sagaut, P., 2000. "Trailing-edge noise prediction using large-eddy simulation and acoustic analogy". *AIAA Journal*, Vol. 38, pp. 575–583.
- Nagarajan, S., Lele, S.K. and Ferziger, J.H., 2003. "A robust high-order method for large eddy simulation". *Journal of Computational Physics*, Vol. 191, pp. 392–419.
- Nagarajan, S., Lele, S.K. and Ferziger, J.H., 2007. "Leading-edge effects in bypass transition". *Journal of Fluid Mechanics*, Vol. 572, pp. 471–504.
- Oberai, A.A., Roknaldin, F. and Hughes, T.J.R., 2002. "Computation of trailing-edge noise due to turbulent flow over an airfoil". *AIAA Journal*, Vol. 40, pp. 2206–2216.
- Sandberg, R.D., Jones, L.E. and Sandham, N.D., 2008. "Direct numerical simulations of noise generated by turbulent flow over airfoils". *AIAA Paper 2008-2861*.
- Sandberg, R.D., Jones, L.E. and Sandham, N.D., 2009. "Investigation and prediction of transitional airfoil self-noise". *AIAA Paper 2009-3104*.
- Singer, B.A., Brentner, K.S. and Lockard, D.P., 2000. "Simulation of acoustic scattering from a trailing edge". *Journal of Sound and Vibration*, Vol. 230, pp. 541–560.
- Wang, M. and Moin, P., 2000. "Computation of trailing-edge flow and noise using large-eddy simulation". *AIAA Journal*,

J.L.F. Azevedo, W.R. Wolf and S.K. Lele
Mach Number Effects on Airfoil Aeroacoustic Sources and Noise Propagation

Vol. 38, pp. 2201–2209.

Wolf, W.R., 2011. *Airfoil Aeroacoustics: LES and Acoustic Analogy Predictions*. Ph.D. thesis, Stanford University.

Wolf, W.R., Azevedo, J.L.F. and Lele, S.K., 2012. “Convective effects and the role of quadrupole sources for airfoil aeroacoustics”. *Journal of Fluid Mechanics*, Vol. 708, pp. 502–538.

Wolf, W.R. and Lele, S.K., 2011a. “Aeroacoustic integrals accelerated by fast multipole method”. *AIAA Journal*, Vol. 49, pp. 1466–1477.

Wolf, W.R. and Lele, S.K., 2011b. “Wideband fast multipole boundary element method: Application to acoustic scattering from aerodynamic bodies”. *International Journal for Numerical Methods in Fluids*, Vol. 67, pp. 2108–2129.

Wolf, W.R. and Lele, S.K., 2012. “Trailing edge noise predictions using compressible large eddy simulation and acoustic analogy”. *AIAA Journal*, Vol. 50, pp. 2423–2434.

7. RESPONSIBILITY NOTICE

The authors are the only responsible for the printed material included in this paper.